Particle size control of a monodisperse spherical Y_2O_3:Eu^{3+} phosphor and its photoluminescence properties

Hyoung Sun Yoo, Ho Seong Jang, Won Bin Im, Jong Hyuk Kang, and Duk Young Jeon[a)]
Department of Materials Science and Engineering, Korea Advanced Institute of Science and Technology, Yuseong-gu, Daejeon 305-701, Korea

(Received 28 November 2006; accepted 10 April 2007)

A monodisperse spherical Y_2O_3:Eu^{3+} phosphor was prepared by a homogeneous precipitation method. The mean size of the phosphor particles (MSPP) was successfully controlled by changing the volume ratio of normal alcohol (RA) (propanol) in the solvents mixed between deionized water and normal propanol. When the RA was increased from 0 to 0.7, the MSPP decreased while maintaining a high yield of >95%. Although the prepared phosphor samples were fired at the same temperature, the thermal energy was delivered more efficiently into the inner side of the phosphor particles with the decrease of the MSPP. Therefore, the crystallinity and also the photoluminescence (PL) intensity of the phosphor increased with the decrease in the MSPP. In addition, because the numbers of Eu^{3+} ions located near the particle surfaces increased with the decrease of particle size, the ratio of PL intensity caused by the $^5D_0$–$^7F_2$ transition to that caused by $^5D_0$–$^7F_1$ transition increased from 10.8 to 12.7 with the decrease in MSPP.

I. INTRODUCTION

Nowadays, high-definition display has been one of the most interesting topics in flat-panel display (FPD) industry. To increase the resolution of a screen, the pixel size of the screen has been continuously reduced. Recent advances in high-definition display have placed some requirements on the development of corresponding phosphors. For application in high-definition displays with small-sized pixels, phosphors with a small size and narrow size distribution are required. A uniform size for the phosphor particles helps to form a uniform thickness of a phosphor layer, and thus their luminescence distribution can be uniform on a whole phosphor screen.[1,2] In addition, phosphor particles should have a spherical shape and high luminescence efficiency. Phosphor particles with a spherical shape are capable of minimizing light scattering on their surfaces. Consequently, the efficiency of light emission and the brightness of a phosphor screen are expected to be improved.[3,4] Another feature of spherical phosphor particles is they can be packed more densely than ones with a different shape so that a dense phosphor layer can be formed by using the spherical phosphor particles.[5–7]

On the other hand, shape and size, and thus luminescent properties, of phosphor particles are strongly affected by the synthesis methods used. It is difficult to control the shape and size of phosphor particles with a conventional solid-state reaction method that requires a high-temperature firing process for a long time as well as mechanical milling processes. Therefore, phosphor particles prepared using a solid-state reaction method have irregular shape and surface damage, which act as a nonradiative transition center and cause a decrease of luminescence efficiency.[8] Recently, a spray-pyrolysis method has been recommended as a promising method with which to prepare fine, spherically shaped phosphor particles. However, the sizes of the phosphor particles prepared with a spray-pyrolysis method are not uniform and have a hollow structure. The hollow structure of the phosphor particles is harmful to mechanical stability and luminescence efficiency.[9,10] Recent progress in a flame spray-pyrolysis method made it possible to prepare solid and nano-sized phosphor particles.[11] On the other hand, Sordelet and Akinc[12] have reported that monodisperse spherical Y_2O_3 particles could be prepared using a homogeneous precipitation method, and the prepared particles did not have a hollow structure but a dense structure. They controlled particle size by changing several parameters, such as the concentration of raw materials, the concentration of urea, and the reaction time. However, at the price of controlling the particle size, they gave up maintaining a high yield of the particles.

In this study, we prepared a monodisperse spherical Y_2O_3:Eu^{3+} phosphor by a homogeneous precipitation

a) Address all correspondence to this author.
e-mail: dyj@kaist.ac.kr
DOI: 10.1557/JMR.2007.0257

method. Furthermore, we controlled the mean size of the phosphor particles (MSPPs) in diameter while maintaining a high yield of >95%. Because the $Y_2O_3:Eu^{3+}$ phosphor is a well-known, highly efficient red-emitting phosphor for use in low-pressure florescent lamps and FPDs such as plasma display panels and conventional cathode ray tubes, it is worthwhile to study the $Y_2O_3:Eu^{3+}$ phosphor.[6–11] In addition, the influences of the MSPPs on the photoluminescent properties of the monodisperse spherical $Y_2O_3:Eu^{3+}$ phosphor were investigated.

II. EXPERIMENTAL

YCl_3–$6H_2O$ (99.99% pure; Aldrich, St. Louis, MO) and $EuCl_3$–$6H_2O$ (99.99% pure; Aldrich) were used as raw materials for sources of Y and Eu ions. In addition, urea (99% pure; Aldrich) was used for homogeneous precipitation. To control the MSPPs, deionized water and a combination of deionized water mixed with normal propanol (99.5% pure; Junsei, Tokyo, Japan) were used as solvents. The total volume of the solvents was fixed, but the various volume ratios of alcohol (RAs)

$$\mathrm{RA} = \frac{\text{Volume of normal propanol}}{\text{Volume of normal propanol} + \text{Volume of deionized water}} \quad , \qquad (1)$$

such as 0, 0.1, 0.2, 0.3, 0.4, 0.5, 0.6, and 0.7 were used in experiments.

After mixing 200 mL of 0.0184 M YCl_3–$6H_2O$ solution and 200 mL of 0.0016 M $EuCl_3$–$6H_2O$ solution for 10 min, 0.15 mols of urea was dissolved in the solution for 5 min. Then the solution was heated to 87 °C and aged for 1 h. The mixed solvents were boiled abruptly at certain temperatures, and as a result the volume of the solution rapidly decreased. When the RA was 0, the temperature was 100 °C, and the temperature as gradually decreased with the increase of the RA from 0 to 0.7. When the RA was 0.7, the temperature was 88 °C. Therefore, the reaction temperature was fixed at 87 °C for all samples to avoid boiling the solvents. About 30 min after the beginning of the aging, the solution began to become white. That meant that at that moment nucleation had occurred, and nuclei were grown into precipitate particles immediately.[13] The precipitate was collected from the aged solution by using a membrane filter (Whatman, Brentford, UK) the mean pore size of which was about 100 nm. Subsequently, the precipitate was washed several times using a solvent that has the same composition as the solvent used in the precipitation reaction. The washed precipitate was dried at 85 °C for 12 h and fired at various temperatures ranging from 750 to 1050 °C for 4 h. The phosphor particles fired at temperatures over 1050 °C were stuck to each other and sintered.

Thermal decomposition characteristics of the precipitate during the firing process were investigated by thermogravimetry (TG)/differential scanning calorimetry (DSC) measurement. TG/DSC measurements were carried out at temperatures ranging from room temperature to 900 °C (DSC) and 1000 °C (TG) at a heating rate of 5 °C/min using a thermal analysis instrument (STA 1500; Rheometric, Reichelsheim, Germany). The morphology and size of the prepared phosphor particles were observed with a Philips XL30SFEG scanning electron microscope (SEM). The MSPP was determined by measuring the diameters of 100 phosphor particles in the SEM image and averaging them. Furthermore, a particle size analyzer (ZetaPlus; Brookhaven Instruments, Holtsville, NY) was used to investigate the MSPPs and the size distribution of the phosphor particles more precisely. The crystalline phases of the phosphor were analyzed by a Rigaku (Tokyo, Japan) D/max–RC x-ray diffractometer with Cu K_α ($\lambda = 1.542$ Å) radiation operating at 40 kV and 45 mA. The scan rate was 1°/min, and the measurement range was from 15° to 65°. Photoluminescence (PL) properties were analyzed by a DARSA PRO 5100 PL spectrometer (Professional Scientific Instrument Co., Suwon, Korea) using a xenon lamp operating at an excitation wavelength of 254 nm. The Brunauer–Emmett–Teller (BET) analysis surface area of the phosphor particles was measured by a surface area and porosity analyzer (ASAP 2020; Micromeritics, Norcross, GA) in a Kr gas atmosphere. In addition, the BET diameter ($d = 6/\rho \times$ the BET surface area) was calculated with taking the density (ρ) of cubic Y_2O_3 as 5.01 g/cm.[3,11] To determine the yield of each phosphor sample, the weight of the fired phosphor sample was measured, and subsequently it was divided by the theoretical weight that could be obtained from the raw materials used.

III. RESULTS AND DISCUSSION

A. Precipitation and crystallization

Figure 1 shows the TG/DSC curves of the dried precipitate powder. Jing et al.[6] have suggested that the composition of the precipitate was amorphous $(Y_{1-x}, Eu_x)OHCO_3$–H_2O. Sordelet and Akinc[12] have suggested that their hydroxycarbonate precipitate underwent two kinds of decomposition reactions and converted to oxide. It was assumed that a similar result was obtained in this work. The precipitate of $(Y_{1-x}, Eu_x)OHCO_3$–H_2O underwent two kinds of decomposition reactions during the firing process as shown in Eqs. (2) and (3), and it changed to the $Y_2O_3:Eu^{3+}$ phosphor:

$$2(Y_{1-x}, Eu_x)OHCO_3 \cdot H_2O \xrightarrow{180^\circ C} (Y_{1-x}, Eu_x)_2O_2CO_3 + 3H_2O + CO_2 \quad , \qquad (2)$$

$$(Y_{1-x}, Eu_x)_2O_2CO_3 \xrightarrow{630^\circ C} Y_2O_3:Eu^{3+} + CO_2 \quad . \qquad (3)$$

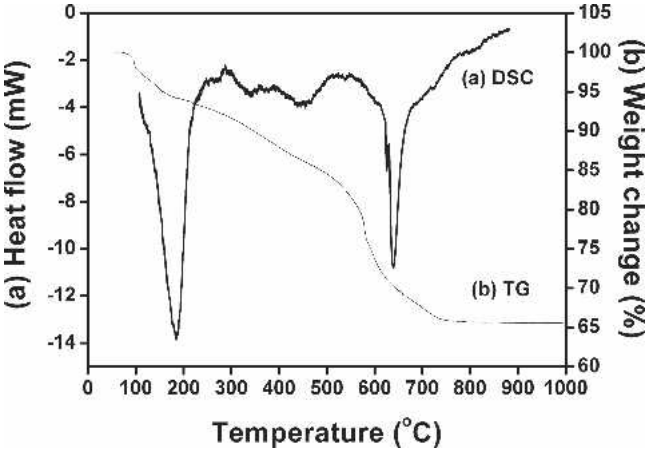

FIG. 1. The (a) DSC and (b) TG curves of the dried precipitate prepared by a homogeneous precipitation method. The measurements were carried out at temperatures ranging from room temperature to 900 °C (DSC) and 1000 °C (TG) at a heating rate of 5 °C/min (RA 0).

The total weight loss was around 34%, which was slightly different from the theoretical weight loss of 38%. It was thought the small difference between the theoretical weight loss and the experimental weight loss was due to a slight deviation in the precipitate composition. It was possible that some portion of H_2O in the $(Y_{1-x}, Eu_x)OHCO_3$–H_2O precipitate was removed during drying at 85 °C for 12 h. Therefore, the experimental weight loss was slightly smaller than the theoretical weight loss. When the RA was 0, the particle size distributions of the dried precipitate and the phosphor obtained after the firing process are shown in Fig. 2. Both the precipitate and the phosphor had small particle sizes and narrow size distributions compared with a commercial Y_2O_3:Eu^{3+} phosphor that was prepared using a conventional solid-state reaction method and was fired at 1400 °C for 5 h. Because byproducts such as CO_2 and H_2O were removed from the precipitate during the firing process, the precipitate was shrunk.[6,12] Consequently, the MSPP was smaller (about 276 nm) than the mean size of the precipitate (about 315 nm). Weight reduction of the precipitate continued to about 750 °C, and there was no additional weight reduction at temperatures higher than 750 °C. This means that all of the byproducts were removed at temperatures under 750 °C and that a temperature of 750 °C was high enough to remove all of the byproducts. Figure 3 shows the MSPP, the BET diameter, and the BET surface area of the prepared phosphor samples at different firing temperatures. Although all of the byproducts were removed at temperatures under 750 °C and there was no additional weight reduction, both the MSPP and the BET diameter decreased with increases in the firing temperature from 750 to 1050 °C. This was caused by an additional densification of the phosphor particles. Although the byproducts were removed at temperatures under 750 °C, the paths of the byproducts remained in the phosphor particles. The additional densification made the paths disappear, and thus the MSPP decreased with an increase of firing temperature.

B. Size control of the monodisperse spherical Y_2O_3:Eu^{3+} phosphor

Figure 4 shows the SEM images of the phosphor samples prepared with various solvents that had different RA values. The phosphor samples had monodisperse spherical shapes. As shown in the inset of Fig. 4(a), particles consisted of many crystallites, and their sizes ranged from 10 to 50 nm. When the phosphor particles were dispersed in the solvent for a particle size distribution analysis, they were well dispersed without strong adhesion among themselves. As shown in Fig. 4, the

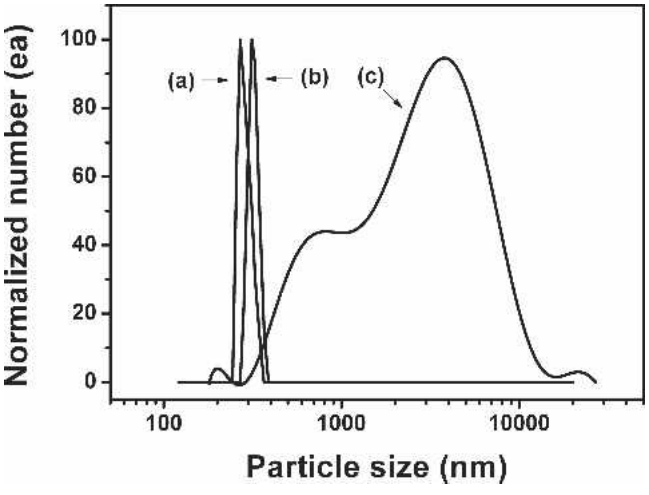

FIG. 2. Particle size distributions of (a) the fired Y_2O_3:Eu^{3+} phosphor at 1050 °C, (b) the dried precipitate, and (c) a commercial Y_2O_3:Eu^{3+} phosphor prepared by a conventional solid-state reaction method (RA 0).

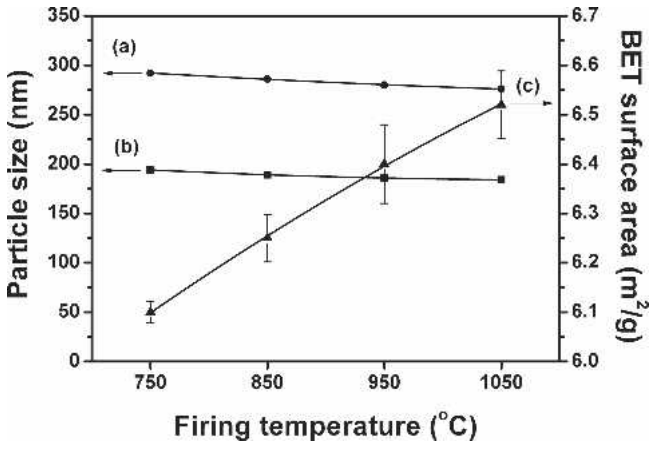

FIG. 3. (a) The MSPP, (b) the BET diameter, and (c) the BET surface area of the monodisperse spherical Y_2O_3:Eu^{3+} phosphor samples prepared at various firing temperatures (RA 0).

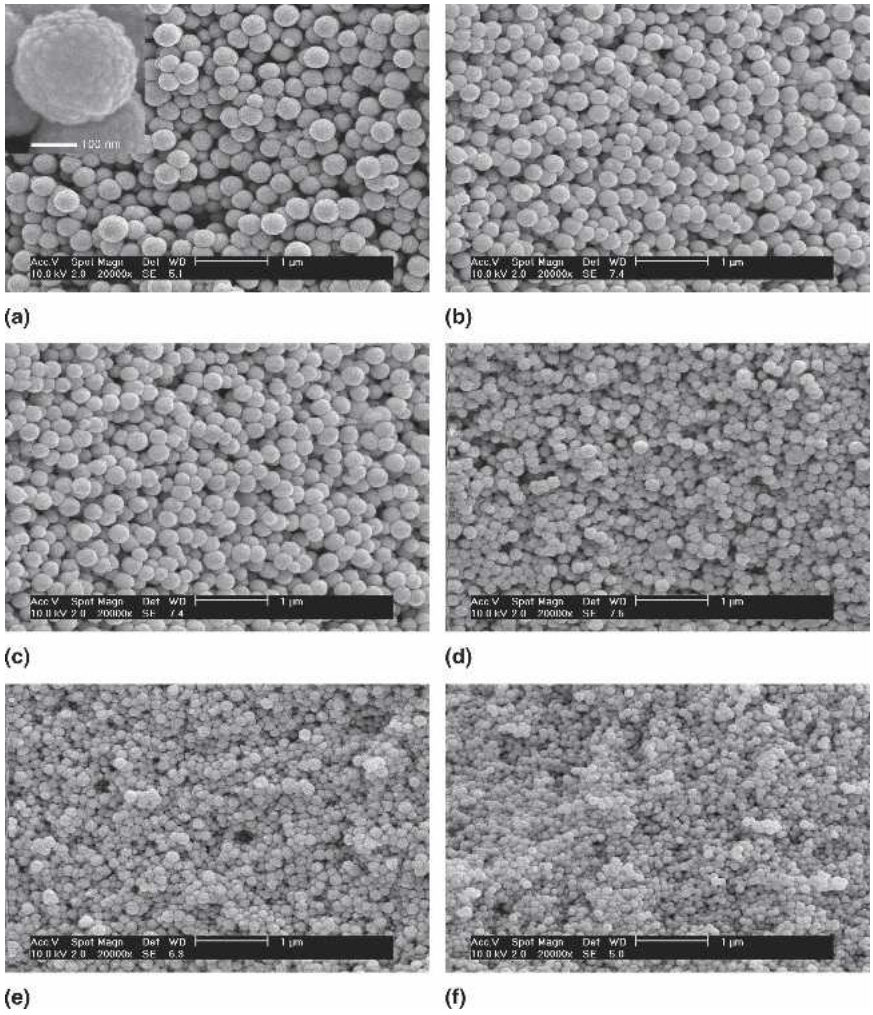

FIG. 4. The SEM images of the monodisperse spherical $Y_2O_3:Eu^{3+}$ phosphor samples prepared with the RA of (a) 0, (b) 0.1, (c) 0.2, (d) 0.4, (e) 0.6, and (f) 0.7. The inset shows the enlarged SEM image of (a) (firing temperature 1050 °C).

MSPP was successfully controlled by changing the RA. Actually, it was possible to control the MSPP by changing the reaction time and the concentration of raw materials.[6,12] In this way, however, it was not easy to obtain a high yield of more than 95%. Because of the insufficient conditions indicated below for the precipitate to fully grow, not all of the raw materials were involved in growth. The MSPP decreased with the decrease in reaction time, and the yield also rapidly decreased.

Sordelet and Akinc[12] reported that when the concentration of Y^{3+} ions was 0.0025 M and the concentration of urea was 0.27 M, the yield decreased from 92.1% to 18.0% with a decrease in aging time from 90 to 10 min. This was because there was not enough time for the precipitate to fully grow. Therefore, some of the raw materials were lost without participation in the precipitation reaction. The MSPP was increased with an increase in the concentration of raw materials, but the yield rapidly decreased. When the concentration of urea was 0.27 M and the aging time was 60 min, the yield decreased from 99.2% to 23.2% with an increase of the concentration of Y^{3+} ions from 0.005 to 0.100 M.[12] That means that the precipitation reaction did not occur efficiently with the increase in the concentration of raw materials.

For the precipitation reaction, the raw materials should be solvated and hydrolyzed. During the solvation and the hydrolysis reaction, water carried out an essential role.[14] In addition, water could help urea to decompose and to provide OH^- and CO_3^{2-}, which participated in the precipitation reaction.[15,16] Therefore, although it was not fully understood, the cause of the decrease in the yield with the increase in the concentration of the raw materials may have been related to an insufficient amount of water. However, the MSPP was successfully controlled by changing the RA while maintaining a high yield of more than 95%. To maintain a high yield for the phosphor, sufficient conditions (i.e., concentrations of raw materials and urea, reaction time, and temperature) should be provided. In this study, the sufficient conditions

were provided, and the particle size was controlled not by the conditions but by the RA. The MSPP, the BET surface area, the BET diameter, and the yield with various RAs are shown in Table I. When the RA was 0 (i.e., only deionized water was used as a solvent), the MSPP of the sample fired at 1050 °C was about 276 nm. It was gradually decreased with the increase of the RA; when the RA was 0.7, the MSPP was about 103 nm. In the cases of the samples fired at 750 °C, the MSPP also decreased from 292 to 109 nm with an increase of the RA from 0 to 0.7. Because the MSPP decreased with an increase of the RA, the BET surface area was increased from 6.52 to 9.00 m^2/g with an increase of the RA. In addition, although the value of the BET diameter was different from the MSPP for each sample, the same tendency was observed. The BET diameter decreased from 184 to 133 nm with an increase of the RA.

The addition of alcohol to pure water alters the dielectric properties of a solvent. Varying the dielectric properties of a solvent affects not only the solubility of the dissolved solute but also the colloidal interaction between solid particles, which would result in changes in the particle size and size distribution.[17] Many researchers have attempted to change the characteristics of metal oxides such as CeO_2,[17] TiO_2,[18,19] and ZrO_2[20,21] by changing the dielectric properties of the solvents. The dielectric constant of the solvent used in this experiment decreased from 80.37 to 31.56 with an increase of the RA from 0 to 0.7.[22] The solubility (C_l), that is the equilibrium concentration of a solute in a saturated solution, can be expressed as[17,23]:

$$C_l \approx \exp\left[-\frac{z^+ z^- e^2}{4\pi\epsilon_0\epsilon_r kT(r^+ + r^-)}\right] , \qquad (4)$$

where the symbols r^+ and r^- represent the radii of ions charged by z^+ and $z-$, respectively; ϵ_0 is the permittivity in vacuum; ϵ_r is the relative dielectric constant of a solvent; k is the Boltzmann constant; and T is the temperature in degrees Kelvin. As can be seen from Eq. (4), the solubility decreased with a decrease in the dielectric constant of the solvent used, which means an increase in the RA. Hu et al.[24] reported that the solubility of ZnO in solvents mixed with water and 2-propanol decreased with an increase in the ratio of 2-propanol. The nucleation rate is closely related to the solubility. The nucleation rate (R_n) can be expressed as[13,17]:

$$R_n = C_0\Gamma \exp\left[-\frac{16\pi\nu^2\gamma^3}{3(kT)^3 (\ln C/C_l)^2}\right] = R_0 \exp\left[-\frac{16\pi\nu^2\gamma^3}{3(kT)^3(\ln C/C_l)^2}\right] , \qquad (5)$$

where C_0 is the initial concentration, Γ is the successful jump frequency of a solute from one site to another, C is the concentration of a solute in a solution, and v is the molecular volume of the solute. γ is the interfacial energy between the precipitate particles and the solution retained; γ decreases with an increase in the volume ratio of alcohols.[17] Because C_0 was fixed in the present experiment, and Γ is almost the same in all cases, R_0 has an almost constant value.[13] If the initial concentration of the solute and the reaction temperature are the same, the homogeneous nucleation rate is mainly affected by the solubility and thus the supersaturation.[13] Therefore, it was easy to be supersaturated with an increase in the RA, and thus the nucleation would occur more easily. For a given concentration of the raw materials, a larger number of nuclei means smaller sized precipitate particles.[13] Therefore, the MSPP decreased with an increase in the RA. Actually, the growth rate could also affect the MSPP. However, the yields of the phosphor samples were higher than 95% in all of the RA values used in the experiments, and that meant that 1 h was long enough for the precipitate to fully grow. In addition, no more increases of particle size were observed 1 h after the beginning of aging. Therefore, we did not have to consider the growth rate. After the initial nucleation takes place in a very short time, the concentration of the solution may be decreased below a specific concentration, which is the minimum concentration for the nucleation.[13] The other solutes, which did not participate in the nucleation process, were involved only in the subsequent growth.[13,25] Consequently, the monodisperse spherical particles were obtained.

TABLE I. Effects of the RA on the MSPP, the BET surface area, the BET diameter, and the yield of the monodisperse spherical Y_2O_3:Eu^{3+} phosphor.

RA	MSPP (nm) 750 °C	MSPP (nm) 1050 °C	The BET surface area (m^2/g)	The BET diameter (nm)	Yield (%)
0	292	276	6.52	184	98.9
0.1	272	257	6.88	174	98.4
0.2	237	224	7.03	170	99.3
0.3	212	200	7.43	161	99.1
0.4	172	163	7.92	151	98.8
0.5	146	138	8.32	144	98.1
0.6	127	120	8.78	136	96.9
0.7	109	103	9.00	133	95.3

The samples fired at 1050 °C were used for the BET analyses.

C. PL properties of the monodisperse spherical Y_2O_3:Eu^{3+} phosphor

Figure 5 shows the x-ray diffraction (XRD) patterns of the monodisperse spherical Y_2O_3:Eu^{3+} phosphor samples prepared with various RA values. The phosphor samples were fired at 750 °C all in the same manner. All of the peaks corresponded to the cubic structure of Y_2O_3, as

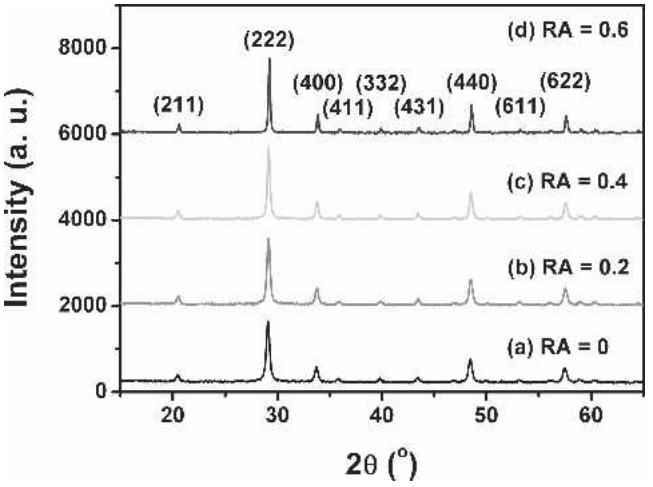

FIG. 5. The XRD patterns of the monodisperse spherical $Y_2O_3:Eu^{3+}$ phosphor samples prepared with the various RA values (firing temperature 750 °C).

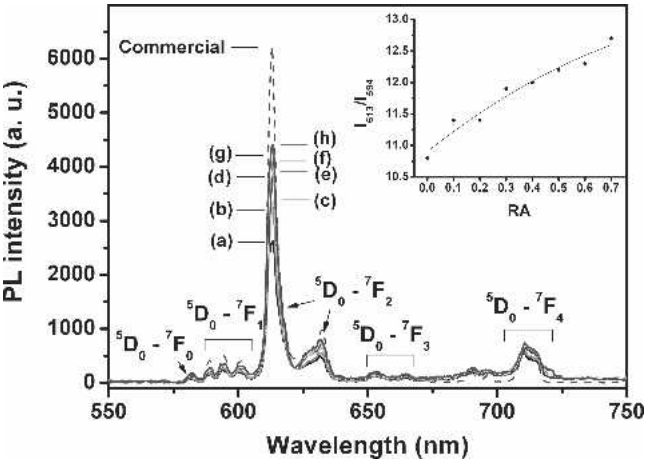

FIG. 6. The PL spectra of the monodisperse spherical $Y_2O_3:Eu^{3+}$ phosphor samples prepared with the RA of (a) 0, (b) 0.1, (c) 0.2, (d) 0.3, (e) 0.4, (f) 0.5, (g) 0.6, and (h) 0.7. The inset shows the PL intensity ratio between two types of transitions (I_{613}/I_{594}) depending upon the RA (firing temperature 750 °C).

indexed in Fig. 5. The intensity, the full width at half-maximum (FWHM) and the area of (222) main peaks in the phosphor samples are shown in Table II. In addition, the crystallite size was calculated from the FWHM of the XRD peak based on Scherrer's formula.[26] The (222) main peak represents the characteristic crystallinity of the $Y_2O_3:Eu^{3+}$ phosphor.[27] The FWHM of the peak decreased and the intensity of the peak increased, and subsequently the calculated crystallite size increased with an increase in the RA. However, the shape of an XRD peak is not related only to the crystallite size. The existence of defects, such as line and plane lattice defects, could cause a broadening of the XRD peak.[28] Therefore, it is not easy to determine a major cause of the sharpening of the peak with an increase of the RA. However, it was thought that thermal energy was delivered more efficiently into the inner side of the phosphor particles with a decrease of the MSPP. In addition, the thermal energy helped the paths of the byproducts to disappear and the crystallite to grow with a decrease of the MSPP. Therefore, the crystallinity of the phosphor increased with a decrease of the MSPP. Figure 6 shows the PL spectra of the monodisperse spherical $Y_2O_3:Eu^{3+}$ phosphor samples prepared with the various RA values. In addition, the PL spectra were compared with that of the commercial phosphor. The PL spectra consisted of the $^5D_0 \rightarrow {}^7F_J$ line emissions of the Eu^{3+} ions, and the main emission peak at a wavelength of 613 nm was due to the $^5D_0 \rightarrow {}^7F_2$ transition. Because the crystallinity of the phosphor increased with an increase of the RA, the PL intensity also increased. However, when the phosphor samples were prepared at 1050 °C, the changes in the crystallinity and the PL intensity depending on the RA values were insignificant.

TABLE II. The intensity, the FWHM, and the area of the (222) main peak in the XRD patterns shown in Fig. 5.

RA	Intensity (a.u.)	FWHM (°)	Area (a.u.)	Crystallite size (nm)
0	1452.9	0.38	1699	25.7
0.2	1582.3	0.35	1538	26.2
0.4	1697.4	0.28	1342	30.9
0.6	1764.5	0.20	1245	41.7

The crystallite size was calculated from the Scherrer's formula[26] (firing temperature 750 °C).

The relative PL intensity among the emission peaks depends on the symmetry of the local environment of the Eu^{3+} activator ions, and it can be described in terms of Judd–Ofelt theory.[29,30] Actually, the magnetic dipole transition of $^5D_0 \rightarrow {}^7F_1$ is permitted and the electric dipole transition of $^5D_0 \rightarrow {}^7F_2$ is forbidden by the parity selection rule. However, in most cases, the local environment of the Eu^{3+} ions does not have inversion symmetry, and the parity-forbidden transition is partially permitted. This relaxation of the selection rule occurs in noninversion symmetry sites, such as C_2 sites occupied by the Eu^{3+} ions in Y_2O_3. When the Eu^{3+} ions occupy the inversion symmetry sites, such as S_6 sites in Y_2O_3, the $^5D_0 \rightarrow {}^7F_1$ transition will appear relatively strong.

Because there are three times more C_2 sites than S_6 sites in Y_2O_3, the Eu^{3+} ions are assumed to occupy these two types of sites with a corresponding ratio.[31] The local symmetry of the sites, which are occupied by the Eu^{3+} ions, can be affected by surface area of the phosphor, because there is a chance that the atoms located near the particle surfaces easily lose their inversion symmetry.[32] The PL intensities at 594 and 613 nm, respectively, were used as the $^5D_0 \rightarrow {}^7F_1$ and the $^5D_0 \rightarrow {}^7F_2$ transitions.[31] The PL intensity ratio of two types of transitions (I_{613}/I_{594}) is shown in the inset of Fig. 6. As

shown in Table I, the MSPP decreased and the BET surface area increased with the increase in the RA. That meant there was a chance that the number of Eu^{3+} ions located near the surfaces of the phosphor particles was increased with an increase in the RA. According to our expectation, the PL intensity ratio showed a tendency to increase from 10.8 to 12.7 with the increase in the RA. It was due to the increase in the number of Eu^{3+} ions located near the particle surfaces, which provided non-inversion symmetry sites. Therefore, as the RA increased, the PL intensity caused by the $^5D_0 \rightarrow {}^7F_2$ transition increased more compared with that caused by the $^5D_0 \rightarrow {}^7F_1$ transition.

IV. CONCLUSION

We prepared a monodisperse spherical Y_2O_3:Eu^{3+} phosphor using a homogeneous precipitation method. The precipitate was thermally decomposed and shrunk during the firing process, and it changed to the cubic Y_2O_3:Eu^{3+} phosphor. Both the precipitate and the phosphor particles were small and had narrow size distributions. The MSPP was successfully controlled by changing the RA while maintaining a high yield of >95%. When the RA was increased from 0 to 0.7, the MSPP of the samples fired at 750 °C was decreased from 292 to 109 nm. The change of the dielectric properties of the solvent affected the nucleation rate, and thus the number of nuclei that were formed during the nucleation process. Because the dielectric constant of the solvent was decreased with the increase in the RA, the number of nuclei was increased and the MSPP was decreased.

Although all of the prepared phosphor samples were fired at the same temperature (750 °C), thermal energy was delivered more efficiently to the inner side of the phosphor particles with the decrease of the MSPP. Therefore, the crystallinity and also the PL intensity of the phosphor increased with a decrease of the MSPP. In addition, the PL intensity ratio between two types of transitions (I_{613}/I_{594}) increased from 10.8 to 12.7 with the increase of the RA. It was due to the increase of the number of Eu^{3+} ions located near the particle surfaces, which provided non-inversion symmetry sites. Therefore, PL intensity at the main emission wavelength of 613 nm caused by the electric dipole transition ($^5D_0 \rightarrow {}^7F_2$) increased more compared with that caused by the magnetic dipole transition ($^5D_0 \rightarrow {}^7F_1$).

REFERENCES

1. G.Y. Hong, B.S. Jeon, Y.K. Yoo, and J.S. Yoo: Photoluminescence characteristics of spherical Y_2O_3:Eu phosphors by aerosol pyrolysis. *J. Electrochem. Soc.* **148,** H161 (2001).
2. S.H. Cho, J.S. Yoo, and J.D. Lee: A new synthetic method to prepare spherical phosphors for emissive screen applications. *J. Electrochem. Soc.* **145,** 1017 (1998).
3. J.S. Yoo and J.D. Lee: The effects of particle size and surface recombination rate on the brightness of low-voltage phosphor. *J. Appl. Phys.* **81,** 2810 (1997).
4. L.D. Vila, E.B. Stucchi, and M.R. Davolos: Preparation and characterization of uniform, spherical particles of Y_2O_2S and Y_2O_2S. *Eur. J. Mater. Chem.* **7,** 2113 (1997).
5. A. Vecht, C. Gibbons, D. Davies, X. Jing, P. Marsh, T. Ireland, J. Silver, and A. Newport: Engineering phosphors for field emission displays. *J. Vac. Sci. Technol., B* **17,** 750 (1999).
6. X. Jing, T. Ireland, C. Gibbons, D.J. Barber, J. Silver, A. Vecht, and G. Fern: Control of Y_2O_3:Eu spherical particle phosphor size, assembly properties, and performance for FED and HDTV. *J. Electrochem. Soc.* **146,** 4654 (1999).
7. T. Hirai, T. Hiranoa, and I. Komasawa: Preparation of Y_2O_3:Eu^{3+} phosphor fine particles using an emulsion liquid membrane system. *J. Mater. Chem.* **10,** 2306 (2000).
8. G. Wakefield, E. Holland, P.J. Dobson, and J.L. Hutchison: Luminescence properties of nanocrystalline Y_2O_3:Eu. *Adv. Mater.* **13,** 1557 (2001).
9. G.Y. Hong, K. Yoo, S.J. Moon, and J.S. Yoo: Enhancement of luminous intensity of spherical Y_2O_3:Eu phosphors using flux during aerosol pyrolysis. *J. Electrochem. Soc.* **150,** H67 (2003).
10. Y.C. Kang, H.S. Roh, and S.B. Park: Preparation of Y_2O_3:Eu phosphor particles of filled morphology at high precursor concentrations by spray pyrolysis. *Adv. Mater.* **12,** 451 (2000).
11. A. Camenzind, R. Strobel, and S.E. Pratsinis: Cubic or monoclinic Y_2O_3:Eu^{3+} nanoparticles by one step flame spray pyrolysis. *Chem. Phys. Lett.* **415,** 193 (2005).
12. D. Sordelet and M. Akinc: Preparation of spherical, monosized Y_2O_3 precursor particles. *J. Colloid Interface Sci.* **122,** 47 (1988).
13. G. Cao: *Nanostructures and Nanomaterials* (Imperial College Press, London, 2004).
14. A.C. Pierre: *Introduction to Sol-Gel Processing* (Kluwer Academic Publishers, London, 1998).
15. J. Silver, T.G. Ireland, and R. Withnall: Fine control of the dopant level in cubic Y_2O_3:Eu^{3+} phosphors. *J. Electrochem. Soc.* **151,** H66 (2004).
16. Y.D. Jiang, Z.L. Wang, F. Zhang, H.G. Paris, and C.J. Summers: Synthesis and characterization of Y_2O_3:Eu^{3+} powder phosphor by a hydrolysis technique. *J. Mater. Res.* **13,** 2950 (1998).
17. H.I. Chen and H.Y. Chang: Homogeneous precipitation of cerium dioxide nanoparticles in alcohol/water mixed solvents. *Colloids Surf., A* **242,** 61 (2004).
18. C.S. Fang and Y.W. Chen: Preparation of titania particles by thermal hydrolysis of $TiCl_4$ in n propanol solution. *Mater. Chem. Phys.* **78,** 739 (2003).
19. H.K. Park, D.K. Kim, and C.H. Kim: Effect of solvent on titania particle formation and morphology in thermal hydrolysis of $TiCl_4$. *J. Am. Ceram. Soc.* **80,** 743 (1997).
20. M.Z.C. Hu, E.A. Payzant, and C.H. Byers: Sol-gel and ultrafine particle formation via dielectric tuning of inorganic salt-alcohol-water solutions. *J. Colloid Interface Sci.* **222,** 20 (2000).
21. J.Y. Choi and D.K. Kim: Preparation of monodisperse and spherical powders by heating of alcohol-aqueous salt solutions. *J. Sol.-Gel Sci. Technol.* **15,** 231 (1999).
22. F. Franks: *Water: A Comprehensive Treatise* (Plenum Press, New York, 1973).
23. J.N. Israelachvili: *Intermolecular and Surface Forces* (Academic Press, London, 1992).
24. Z. Hu, G. Oskam, and P.C. Searson: Influence of solvent on the growth of ZnO nanoparticles. *J. Colloid Interface Sci.* **263,** 454 (2003).
25. M. Haruta and B. Delmon: Preparation of homodisperse solids. *J. Chem. Phys.* **83,** 859 (1986).

26. W. Zhang, M. Xu, W. Zhang, M. Yin, Z. Qi, S. Xia, and C. Garapon: Site-selective spectra and time-resolved spectra of nanocrystalline Y_2O_3:Eu. *Eur. Chem. Phys. Lett.* **376,** 318 (2003).
27. S.H. Byeon, M.G. Ko, J.C. Park, and D.K. Kim: Low-temperature crystallization and highly enhanced photoluminescence of $Gd_{2-x}Y_xO_3:Eu^{3+}$ by Li doping. *Chem. Mater.* **14,** 603 (2002).
28. P. Scardi and M. Leoni: Fourier modeling of the anisotropic line broadening of x-ray diffraction profiles due to line and plane lattice defects. *J. Appl. Crystallogr.* **32,** 671 (1999).
29. B.R. Judd: Optical absorption intensities of rare-earth ions. *Phys. Rev.* **127,** 750 (1962).
30. G.S. Ofelt: Intensities of crystal spectra of rare-earth ions. *J. Chem. Phys.* **37,** 511 (1962).
31. G. Blasse and B.C. Grabmaier: *Luminescent Materials* (Springer-Verlag, Berlin, 1994).
32. Z.G. Wei, L.D. Sun, C.S. Liao, X.C. Jiang, and C.H. Yan: Synthesis and size dependent luminescent properties of hexagonal $(Y,Gd)BO_3$:Eu nanocrystals. *J. Mater. Chem.* **12,** 3665 (2002).